ELSEVIER

Marine Geology 246 (2007) 123 – 143

MARINE GEOLOGY
INTERNATIONAL JOURNAL OF MARINE GEOLOGY, GEOCHEMISTRY AND GEOPHYSICS

www.elsevier.com/locate/margeo

Evidence of sediment resuspension by nonlinear internal waves on the western Portuguese mid-shelf

Luis Santos Quaresma [a,*], João Vitorino [a], Anabela Oliveira [a], José da Silva [b]

[a] *Instituto Hidrográfico, Rua das Trinas, 49, 1249-093 Lisboa — Portugal*
[b] *Department of Physics and Institute of Oceanography, Faculdade de Ciências da Universidade de Lisboa, Campo grande 1700 Lisboa — Portugal*

Accepted 13 April 2007

Abstract

In-situ observations of nonlinear internal waves (NIWs) propagating over the northern shelf of Portugal, near the Nazaré submarine canyon (39°47.4′N/009°11.4′W), and evidence of their action on the bottom, are presented and discussed. Synthetic Aperture Radar (SAR) images from this margin suggest the generation of NIWs over the canyon head (39°35′N/009°25′W) and the subsequent propagation directly to the mid-shelf. An observational program was conducted in this area in the summer of 2004, between August 29th and September 1st, to study these short-period internal waves. Temperature and current high resolution measurements were made with thermistor chains and acoustic Doppler current profilers (ADCPs), moored along the canyon generated NIW track, at the 82 m isobath. A simultaneous ENVISAT SAR image was obtained during the experiment. These observations were complemented by a CTD survey and bottom sediment sampling. Collected data show the propagation of large amplitude internal solitons forcing strong bottom current pulses. Turbidity profiles and ADCP echo variability suggest the remobilization of the mid-shelf bottom sediments induced by these short-period events. Calculations of bottom shear stress, induced by the observed canyon generated NIWs, reveal an energetic internal wave activity that can complement, during summer, the role of winter swell in sediment resuspension over the mid-shelf. This work is a contribution to the European project EUROSTRATAFORM, whose objectives include the study of the specific canyon systems dynamics and related sedimentary impacts on the European continental margin.
© 2007 Elsevier B.V. All rights reserved.

Keywords: Nazaré submarine canyon; Portuguese mid-shelf; nonlinear internal waves; bottom shear stress; Shields parameter; sediment resuspension

1. Introduction

Internal waves are ubiquitous dynamic features present inside the stratified ocean. They are commonly generated over continental margins, where strong currents and stratification coexist over irregular topography, with frequencies that span from the local Coriolis to the maximum buoyancy of the water column (Kantha and Tierney, 1997). This means that it is possible to observe, within the ocean, internal oscillations as inertial waves, internal tides and short-period nonlinear internal solitons (Huthnance, 1995). These density perturbations can propagate over large distances and transport mass and momentum, forcing considerable velocity shear that

* Corresponding author. Tel.: +351 210943000; fax: +351 210943299.
E-mail address: luis.quaresma@hidrografico.pt (L.S. Quaresma).

0025-3227/$ - see front matter © 2007 Elsevier B.V. All rights reserved.
doi:10.1016/j.margeo.2007.04.019

can lead to turbulence and mixing (Staquet and Sommeria, 2002). They also can force enough bottom shear stress to suspend sediments over the continental shelf and slope regions (Cacchione and Southard, 1974; Bogucki et al., 1997; Noble and Xu, 2003), contributing to the formation of bottom nepheloid layers (Cacchione and Drake, 1986; Puig et al., 2004).

The nonlinear internal waves (NIWs), known as *solitary internal waves* or *solitons*, owe their existence to an exact balance between nonlinear steepening of the wave form and the tendency toward linear wave dispersion (Benney, 1966). This balance maintains the shape and speed of the solitons as they propagate into internal density frontiers (Vlasenko et al., 2005). These short-period pycnocline fluctuations (tens of minutes) correspond predominantly to singular downward displacements, in the form of a KDV equation solution (Liu and Chang, 1998). Their amplitudes vary from a few to tens of meters and their maximum wavelengths from 100 to more than 1000 m. Typically, these solitons appear in nature grouped in wave trains, rank-ordered by amplitude (with the largest at the front of the train and the smallest at its rear — *canonical behavior*), as the speed of each wave is an increasing function of its amplitude (Apel, 2003).

NIWs are often observed in temperature, salinity and velocity records (even in planktonic layer displacements, Lennet-Cody and Franks, 2002). However, it is the remote sensing, both radar and optical, that shows the world wide manifestation of these features, mainly over the continental margins (Jackson and Apel, 2002; Jackson, 2004). Previous studies based on Synthetic Aperture Radar (SAR) images and *in-situ* measurements revealed the existence of a strong NIW activity over the western Portuguese shelf, especially during the summer season (Da Silva, 1997; Da Silva et al., 1998; Jeans and Sherwin, 2001a,b; Sherwin et al., 2002; Small, 2002). These studies suggest a continental shelf-break generation of NIW solitons by semi-diurnal tidal currents. Once generated, these solitary waves tend to propagate shoreward and reach the mid-shelf grouped in thermocline fluctuation packets.

Recent analysis of SAR images from the western Portuguese margin revealed the near shore generation of NIWs, over the Nazaré submarine canyon head (39°35′N/009°25′W), as well as the subsequent propagation of these waves directly to the mid-shelf (Quaresma, 2006). These unusual characteristics (canyon generation and shallow water propagation), motivated the conduction, in summer 2004, of an observational program of these nonlinear internal processes, in order to study their dynamics and possible impacts on the bottom sedimentary cover.

The aim of this paper is to discuss the role that NIWs generated at the Nazaré submarine Canyon rim (C-NIW) may play in sediment resuspension, over the western Portuguese mid-shelf and to propose a mechanism for bottom nepheloid layer formation, observed by Oliveira et al. (2007-this issue) in this area, during summer.

2. Regional settings

2.1. Oceanography

The western Portuguese shelf dynamics exhibit a seasonal pattern modulated by the evolution of two major atmospheric systems, the Azores High and the Iceland Low (Wooster et al., 1976). During winter, when the anticyclone is displaced to its most southern position and the Iceland Low is reinforced, strong south-westerly winds establish a downwelling regime over the shelf. Typical winter storm events induce a highly energetic wave regime, with significant wave heights exceeding 5 m (Vitorino et al., 2002a). During summer, due to the migration of the Azores High to the central North Atlantic (offshore the Iberian Peninsula) and the simultaneous weakening of the Iceland Low, upwelling favorable northerly wind events dominate. This regime leads to the development of a surface equatorward jet (Fíúza et al., 1982) that extends vertically, from surface to bottom, with the persistence of each northerly wind event (Jorge da Silva, 1992). This summer regime lasts from March to October (Wooster et al., 1976), and is accompanied by low energy wave conditions, with typically significant wave heights of about 2 m (Pires, 1989).

The water column stratification also shows a seasonal evolution, reflecting the seasonal character of the atmospheric forcing. During winter, surface cooling and mixing, promoted by storm events, lead to the homogenization of the shelf waters to depths of about 100 m (Vitorino et al., 2002a). During summer, the increasing solar radiation energy flux and low wave energy regime reduces the mixing effectiveness and generates seasonal upper layer stratification, reinforced by the arrival of cold upwelled waters (Jorge da Silva, 1992).

The shelf tides are dominated by the M_2 semi-diurnal constituent and mainly modulated over one moon cycle by the S_2 semi-diurnal constituent (Sauvaget et al., 2000). The tidal harmonics propagate from south to north as Kelvin waves, with amplitudes increasing towards the coast (Fanjul et al., 1997). The tidal current ellipses are polarized with the bathymetry (Fortunato et al., 2002) and show amplitudes rarely above 0.2 m s^{-1} (Taborda, 1999; Sauvaget et al., 2000). Although, the tidal flow is mainly barotropic, significant three-dimensional hydrodynamic

features can be induced by water column stratification, with the interaction of the tidal current with the continental slope (Quaresma, 2000a; Quaresma et al., 2000; Clemente et al. 2000).

2.2. Mid-shelf sediment dynamics

The importance of physical forcing for the sediment dynamics over the western Portuguese shelf, north of the Nazaré canyon, has been discussed and quantified in several complementary studies (Taborda, 1999; Vitorino et al., 2000b; Jouanneau et al., 2002; Oliveira et al., 2002). The fine sediment resuspension events, over the mid-shelf, are reported by these authors mainly as a result of high bottom shear stress induced by storm waves, observed during winter. Such events intensify the bottom nepheloid layer (BNL) that covers the entire continental shelf (Oliveira et al., 2002).

During summer regime, the suspend particulate matter concentration is generally characterized by low values over the shelf (<2.0 g m^{-3}), with a BNL ranging in thickness from 10 to 20 m, occurring as far as to the shelf-break and with increasing turbidity over the mid-shelf fine deposits (Oliveira et al., 2007-this issue). However, the physical generation mechanism of this summer BNL is not fully understood. The low wind wave energy environment, characteristic of the summer conditions, has little effect on the sedimentary cover at mid-shelf depths (Vitorino et al., 2002b; Taborda, 1999). On the other hand, low-frequency current observations show that they are too weak to promote resuspension, but strong enough to transport the

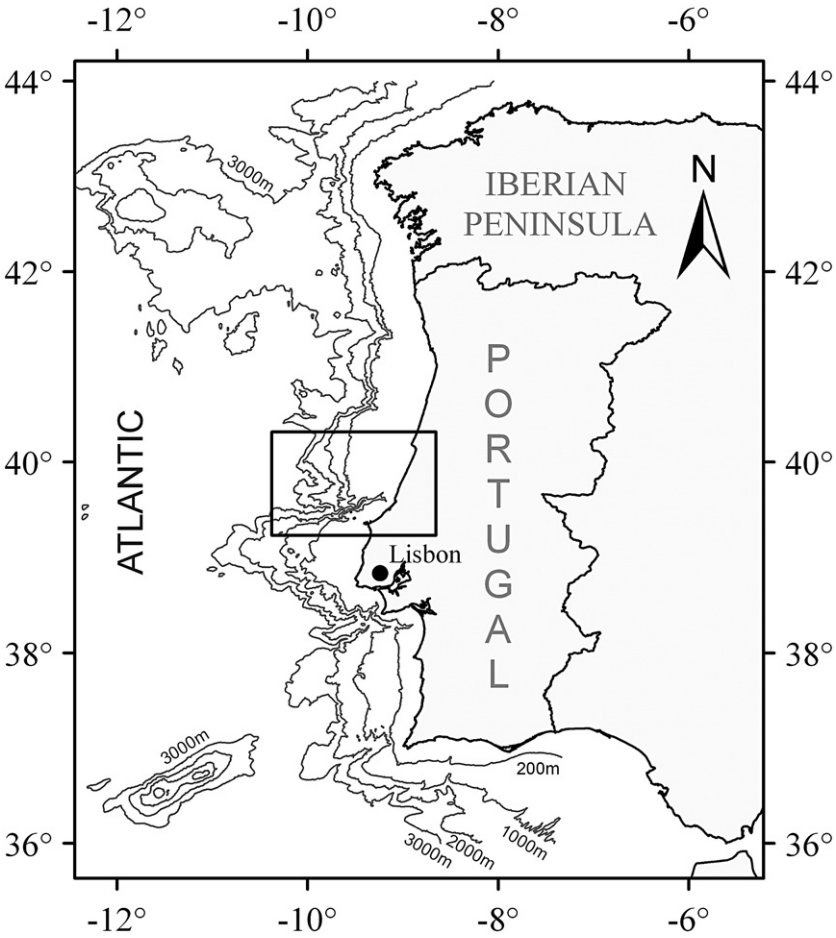


Fig. 1. The Nazaré submarine canyon region and study area (inset). The canyon zone extends about 270 km and completely cuts the western Portuguese continental margin. The canyon head is situated at the coast, in the Nazaré bay and the canyon ends in the deep Eastern North Atlantic. South of the canyon the continental shelf extends offshore in a large plateau (*Estremadura spur*) and in the north, the shelf is rather regular and narrow (40–50 km).

suspended sediment (Taborda, 1999). During upwelling events this transport occurs southward and shoreward, in the bottom Ekman layer (Vitorino et al., 2002b).

2.3. The Nazaré canyon

The Nazaré submarine canyon is one of the largest of the world, cutting the western Portuguese continental margin from the deep ocean to the coastline, and extending for about 270 km (Vanney and Mougenot, 1990). North of the canyon, the shelf is narrow (40–50 km) and flat, with an average bottom slope of about 0.003 (Vanney and Mougenot, 1981). Both topography and coastline are generally oriented along a SW–NE direction. South of the canyon, the shelf becomes narrow and shallow, being confined between Cape Carvoeiro (Peniche) and the Berlengas Islands (Fig. 1).

The sedimentary cover on the shelf north of the canyon shows a sub-parallel bathymetric development of some main deposits (Dias, 1987; Duarte, 2002; Oliveira et al., 2007-this issue), being composed by: an inner mid-shelf area (less than 50 m water depth) formed by fine well sorted sands (150–200 μm); a mid-shelf zone (50–90 m depth) of coarse sand and gravel (see Section 5.1); and a mid-outer shelf muddy region (90–120 m depth) where the finer silt particles dominate. The mid-shelf sandy-gravel deposit is interpreted as remains of a paleo-littoral sedimentary sequence (Pombo, 2004) that should tend to be covered by recent fine sandy sediments due to present day deposition. However, bottom sediment sampling surveys and seismic data show that this deposit, over the north canyon mid-shelf (Fig. 2), is actually irregular relatively to the surrounding, due to a lack in fine sand deposition (Rodrigues, A., personal communication). This behavior suggests the presence of hydrodynamic

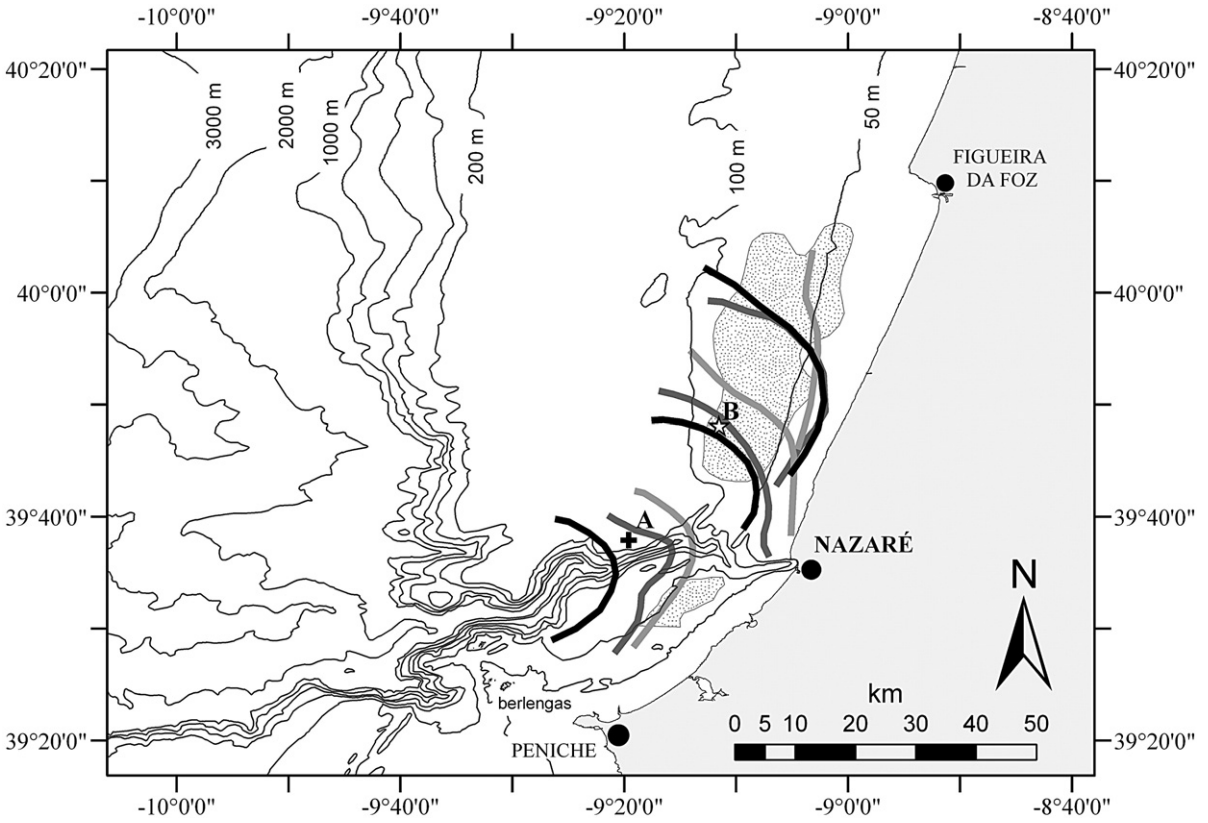


Fig. 2. Spatial evolution of C-NIW trains over the Portuguese continental mid/inner shelf (C-NIW activity area). The bold lines correspond to surface manifestations of the C-NIW solitons. The figure is a composition of three different ERS2 SAR images, covering different tidal phases (observed at Nazaré port tide gauge): in black the ERS2 from 17AUG2003 (low tide); in dark grey the ERS2 14JUL1999 (low tide+2 h); in light grey the ERS2 from 27AUG2003 (low tide+3 h). Each SAR image contributes with three different C-NIW soliton signatures. The most western soliton signature is over the C-NIW generation spot and the most eastern is near the C-NIW breaking depth. Also shown are the position of both observational stations (A and B) and the mid-shelf sandy-gravel deposits represented as the grey dots area, adapted from Pombo (2004).

processes that inhibit the deposition of fine sediments and/or promote their erosion.

As a giant topographic feature, the Nazaré canyon plays an important role over the regional water mass circulation. The canyon promotes a significant water mass and energy exchange between the inner shelf and the deep ocean. The canyon axis configuration seems to force a baroclinic energy convergence (into it) and a barotropic energy divergence (to the adjacent shelves). As a result, a strong semi-diurnal internal tide is observed inside the canyon (Quaresma, 2000a), as well as the decrease of the barotropic tidal amplitude over the canyon head (Sauvaget et al., 2000). Observations reveal that this large amplitude internal tide (>40 m) transports a significant amount of potential energy in the internal density perturbation. The same data showed that this energy is being dissipated along the upper canyon rim, possibly to higher frequency internal oscillations like NIWs (Quaresma, 2000). Large NIW signatures were in fact observed in satellite imagery by Alpers (1985), in the region of Nazaré Canyon.

3. Remote sensing evidence of NIW at Nazaré

Ocean internal waves are commonly visible in SAR remote sensing as groups of quasi-periodic parallel bands impressed on a grey background. This is due to the modulation of the surface capillary waves by the internal wave orbital velocity field (Alpers, 1985; Da Silva et al., 1998).

The present work started with the use of remote sensing techniques to evaluate the generation of NIWs over the Nazaré upper canyon, proposed earlier by Quaresma (2000). A set of 10 chosen ERS-1 and ERS-2 SAR images, taken over the Nazaré coastal region (from 1994 to 2002), were used to observe the spatial evolution of NIWs activity. The radar signatures of these waves show the propagation of two different groups of NIWs, with different origins and different tracks. The most common group is observed to cross the shelf with an eastward direction, presumably generated at the continental shelf-break (SB-NIWs). The other group appears frequently over the upper canyon axis, in a region where the canyon valley shows a strong width reduction (39°37′N/009°23′W). These *Canyon generated NIW* (C-NIW) surface manifestations show a very small curvature radius, suggesting a nearby generation site, over the upper Canyon rim. The changing topography of the canyon head region seems to force the deformation of the soliton fronts due to refraction processes. As a result, each C-NIW packet is divided in two by the canyon axis (with different wave numbers and phase speeds). From these two, the most persistent is the poleward wave train that propagates almost parallel to the shoreline, along the mid-shelf (Fig. 2). Refraction processes along the propagation path lead to a re-orientation of these C-NIW trains, which become almost parallel to the shoreline, along the 50 m isobath. This behavior limits the region of activity of the C-NIWs from the canyon axis to about 40°05′N latitude.

In most cases, it is possible to identify in the same SAR overpass different trains of C-NIWs, propagating along the poleward track. Each train corresponds to successive semi-diurnal C-NIWs generation events (Fig. 2), and is separated from its predecessor by an internal tide wavelength (of about 20 km).

4. *In-situ* observations of C-NIWs (2004 experiment)

The strong surface manifestations and the near shore propagation of the C-NIW trains, identified in SAR imagery (see Section 3), encouraged the implementation of an observational program, aiming to provide a set of measurements to characterize these structures and appraise their impact on the local bottom sediment. This program was held from August 29th to September 1st 2004 onboard NRP *AURIGA*, a 30 m long research vessel of the Portuguese Navy. The observations were conducted during spring tide and at the end of a typical summer upwelling event. During the entire experiment the surface wind wave regime was negligible, with significant wave heights smaller than 2 m and periods varying from 8 to 10 s (Quaresma, 2006).

Two observational stations were settled along the C-NIWs track, at 140 and 82 m depths (mid-shelf). The first observational station (*Station A*, see Fig. 2) was placed over the canyon rim, located near the C-NIWs generation spot (39°38.2′N–009°19.8′W). This mooring was composed by one 100 m Aanderaa thermistor chain and two Aanderaa acoustic currentmeters (RCM9). The chain was set to measure the temperature profile from 10 to 100 m depth (corresponding to 130–40 m above bottom) with a vertical resolution of 10.0 m and a sampling interval of 1 min. The currentmeters were placed at 25 and 55 m depth (115 and 85 mab) and set to record every minute. The strong buoyancy distributed along the mooring cable granted a stable measurement, resulting in a maximum inclination of less than 10° (confirmed by pressure records) which lead to a maximal vertical displacement of about 2 m.

The second observational station (*Station B*, see Fig. 2) was placed over the mid-shelf sandy-gravel deposit, in a sediment body dominated by sand (39°47.4′N–009°11.4′W). This mooring was composed of two Aanderaa thermistor chains (20 m each) and two Aanderaa RCM9 currentmeters (Fig. 3). The chains were set to measure the

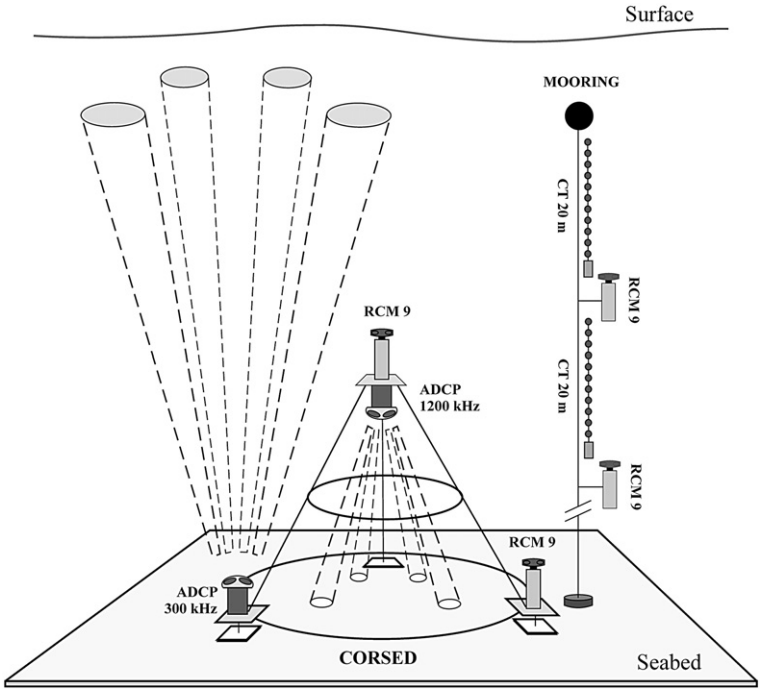


Fig. 3. NIWs recording *Station B* (39°47.4′N/009°11.4′W). This station was deployed along the C-NIW track, at 80 m depths (mid-shelf). It was composed by a 5 m tripod (CORSED) and a mooring. The tripod carried two ADCPs (an upward-looking 300 kHz and a downward-looking 1200 kHz) and 2 acoustic currentmeters (RCM9). The mooring carried two thermistor chains (CT 20 m) and two currentmeters (RCM9), placed between 12 and 60 m depth (corresponding to 70–22 m above bottom). All the equipments were set to record at a sampling interval of 1 min.

temperature profile, from 12 to 55 m depth (70–27 mab), with a vertical resolution of 2.0 m and at a sampling interval of 1 min. The currentmeters were placed at 33 and 60 m depth (49 and 22 mab) and set to record every minute. The strong buoyancy distributed along the mooring cable granted a stable measurement, resulting in a maximum inclination of less than 10° (confirmed by pressure records) which lead to a maximal vertical displacement of about 1 m.

Within a short distance from this second mooring (about 50 m away) a current profile monitoring tripod was deployed. The CORSED tripod, developed by Quaresma et al. (2003), was equipped with an upward-looking and a downward-looking RDI acoustic Doppler current profiler (ADCP), as well as two RCM9 currentmeters (Fig. 3). The upward-looking was a 300 kHz ADCP set to measure the velocity profile from the near bottom layer (4.0 mab) to the near-surface region (about 4 m depth), with a vertical resolution of 2.0 m. The downward-looking was a 1200 kHz ADCP placed at the top of the tripod (5.0 mab) and set to measure the bottom layer velocity profile (0.4–4.3 mab), with a vertical resolution of 0.15 m. Both ADCPs were set to record at a sampling interval of 1 min. Each recorded ensemble resulted from an average of 200 pings (filtering the surface wind wave orbital velocities). The CORSED structure configuration originated an acoustic contamination from 3.0 to 3.5 mab and from 4.5 to 6.5 mab (filled by polynomial interpolation). Since the bottom reflection contaminates the first two downward-looking ADCP bins, the closest velocity measurement (to the bottom) was centered at 0.4 mab.

To complement these measurements, a hydrographic survey along the C-NIWs track was performed (Fig. 4) in order to ascertain the hydrographic conditions of the domain (stratification and turbidity). This observational component was carried out by an IDRONAUT-320 CTD (20 Hz sampling rate) dropped and hoisted at the average speed of 1 m s^{-1}. The hydrographic profiles were performed from 5 m depth to 5 mab. Continuous CTD yo-yo profiles were also performed over three different positions along the C-NIWs track, while the ship was held on station during ~60 min (Fig. 4). Two bottom sediment samples were taken near the deployment site *B* (using a Smith McIntyre grab) in order to characterize the nature of the bottom sediment. An ENVISAT SAR image, from the Nazaré area, was acquired in Image Precision Mode for the period of the

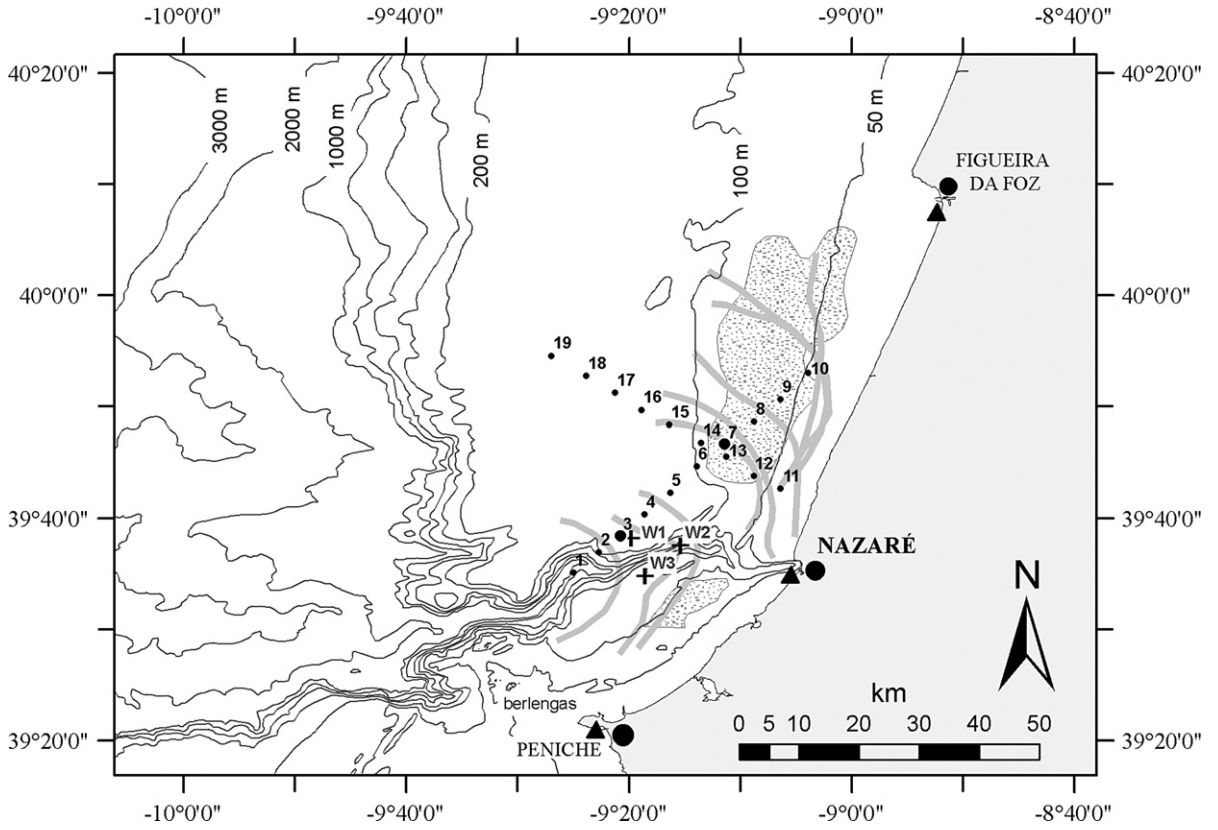


Fig. 4. Location of the hydrographic CTD profiles (black dots), CTD yo-yo profiles (crosses), tide gauges (triangles) and the mid-shelf sandy-gravel deposits (grey dots area). Light grey lines indicate the spatial evolution of C-NIW trains over the Portuguese continental mid/inner shelf (Fig. 2). Note that CTD profile no. 3 is placed over *Station A* and the CTD profile no. 7 is placed over *Station B*.

experiment (30th of August at 10:54 UTC). Finally, three tide gauges recorded the water height at the coast, along the C-NIWs activity area (Fig. 4).

In this paper we focus our attention on the results from *Station B* and from remote sensing image analysis, as the present aim is to discuss the characteristics of C-NIWs over the mid-shelf and to appraise their bottom sediment impact. A more detailed analysis of the complete data set, aiming at the physical process of the propagating internal waves is subject of another article, in preparation by the authors.

5. Background conditions

5.1. Bottom sediments

The sandy-gravel deposit shown in Fig. 2 is limited by the 90 and 40 m isobaths and occupies the coastal margin between the canyon head and 40°05′ latitude (Pombo, 2004). Inside this deposit, small sediment bodies dominated by sand were observed by Duarte (2002). Observational *Station B* was placed over one of these sandy sediment bodies, at 82 m depth (Fig. 2). The seabed sediment samples taken at this site revealed a non-cohesive sediment (<1% of clay), mainly composed by sand (up to 93%), with a small fraction of clay and silt (6%), and gravel (1%). The grain size distribution of the bed surface sediments (0.1 m deep) is shown in Fig. 5. The main modal size is of about 214 μm (sand) and the grain size distribution is represented in Table 1.

5.2. Water column stratification

The CTD profiles obtained during the observational program were used to characterize the background stratification conditions in the study area. Typically they show a two-layer stratified system, with a strong near surface seasonal thermocline (15 m thick) centered at about 15 m depth. This internal temperature frontier separated a well mixed upper layer of warm water (17 °C) from a lower layer of colder waters (of about 14 °C). Fig. 6 shows the undisturbed density profile (γ_T), obtained near *Station B* (39°45.6′N–009°11.3′W, on the 29th of August at 23:45 UTM) and the corresponding smooth *buoyancy*

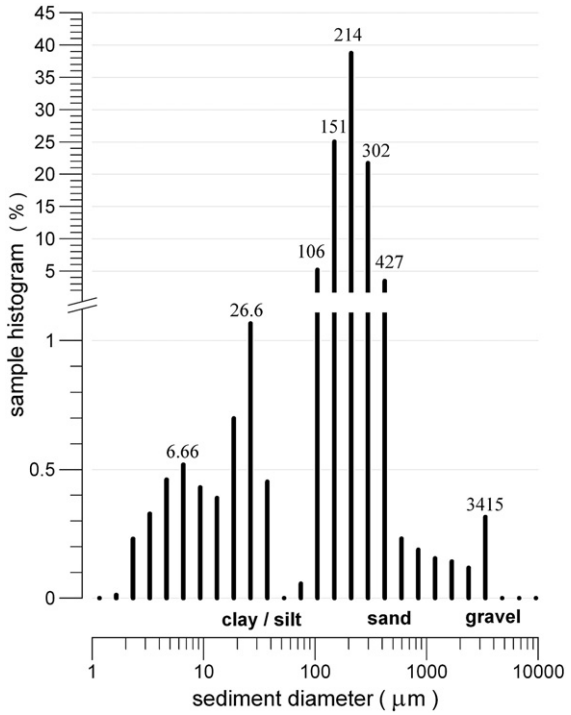


Fig. 5. Grain size distribution of the collected seafloor sediment samples (0.1 m deep) at *Station B* (see location in Fig. 2). Bars are labeled by means of sediment diameter (μm) of the corresponding grain size class (see Table 1).

frequency profile, *N* (filtered by a running mean of 5 m). *N* attains a maximum of 14 cph at 10 m depth (pycnocline) and decreases towards the surface and bottom. These stratification conditions can be simplified as a two-layer model, with an upper layer density of about 1026 kg m^{-3} and a lower layer density of about 1027 kg m^{-3}. It is important to note that this stratification (both thermocline depth and lower mixed layer height) results from the stage of the upwelling process. Note also that the well mixed lower layer indicates a mature stage of this process, characteristic of the middle summer season over the Portuguese continental shelf.

6. NIW experiment observations

6.1. SAR image

The SAR image available for the survey period revealed a complex internal wave activity over the north canyon shelf region (Fig. 7). The two main groups of NIW discussed in Section 3 are observed in the SAR image and both sets of soliton signatures seem to reproduce the same track direction identified earlier. Over *Station B* there is evidence of a crossing-over event of these two different wave trains: the shelf-break (SB-NIW) and the canyon (C-NIW) generated waves. As a result of this process, the mid-shelf is almost completely covered by NIWs (Fig. 8).

6.2. Temperature profiles

The thermistor chain measurements show, throughout the experiment, large amplitude (10–30 m) short-period (8–25 min) fluctuations of the thermocline. The amplitude/period characteristics of these fluctuations suggest that they corresponded to short-period depression solitons, grouped by wave packets (Fig. 9a), similar to the KdV solution. Each packet is separated by a semi-diurnal tidal period, suggesting a tidal generation. In fact, these NIWs seem to be generated at the beginning of the barotropic flood tide period (observed by the tide gauge mounted at the port of Nazaré), crossing *Station B* half a day later. The complete temperature profile time series revealed a disturbed version of the wave train *canonical picture* (see Section 1), with changing time gaps between consecutive solitons and no observation of an amplitude rank-order (inside each soliton packet). This behavior is probably due to the crossing-over event observed in the SAR image (see Section 6.1), therefore being the result of two different NIW trains (C-NIW and SB-NIW).

6.3. Current profiles

The current profile time series, obtained by the ADCPs, show the current structure associated with the thermocline fluctuations (see Section 6.2). The velocity profiles obtained with the upward and downward-looking ADCPs were coupled in order to produce a synthesized profile set, ranging from bottom (0.4 mab) to near surface (4 m depth). The complete profile time series (both vertical and eastward velocity component)

Table 1
Main grain size distribution of the collected seabed sediment samples (0.1 m deep) at *Station B* (see location in Fig. 2)

Sediment grain size class (μm)	Mean sediment diameter (μm)	Sample abundance (%)
4000–1000	2500	0.8
500–354	427	3.5
354–250	302	21.7
250–177	214	38.8
177–125	151	25.0
125–88.4	106	5.2
44.2–31.2	37.2	0.5
31.2–22.1	26.6	1.1
22.1–15.6	18.6	0.7
15.6–0.98	8.3	3.3

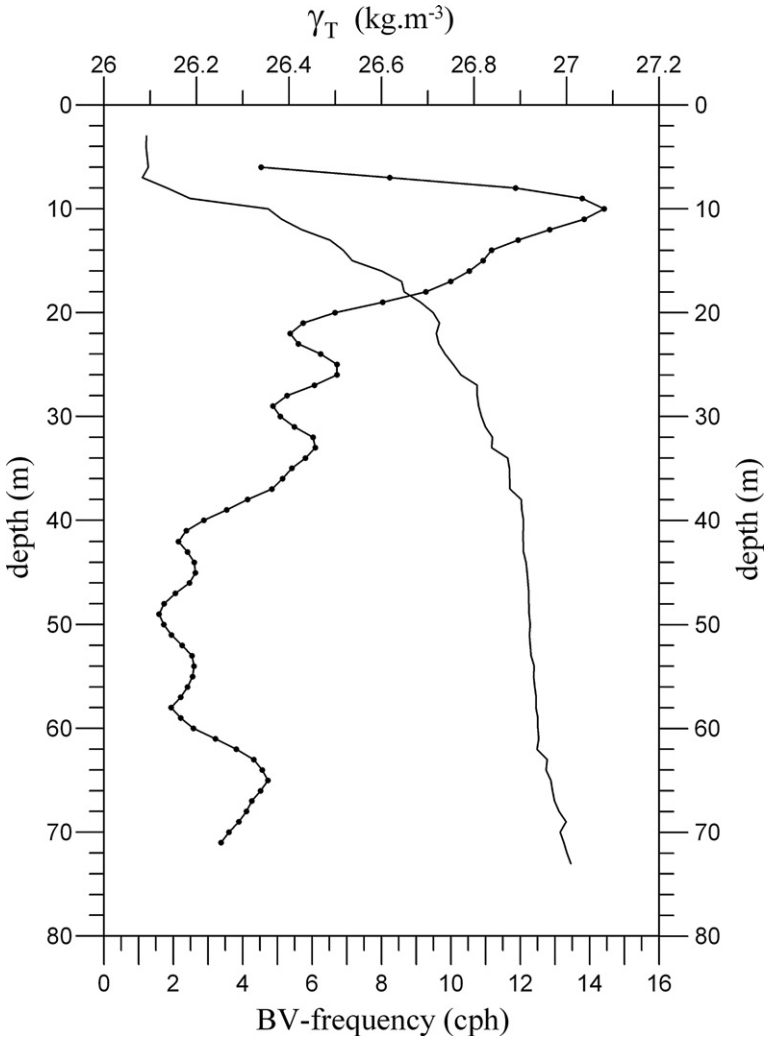


Fig. 6. CTD profile no. 13 (see location in Fig. 4), obtained on the 29th of August at 23:45 UTM. The line shows the density profile, γ_T, and the dotted line shows the corresponding smoothed buoyancy frequency profile, *N*, processed with a running mean filter (5 m length).

show several short-period current pulses, which are in phase with the short-period thermocline depressions. These features are visible in the time series section presented in Fig. 9a, c. The solitons are particularly well expressed in the vertical component, where each NIW produces a bipolar structure, ranging from −0.1 to 0.1 m s^{-1}, in a short 15 min interval (Fig. 9b).

The spectra of the eastward and northward velocity components evidence two energetic frequency bands, separated by a low energy field at the period of about 5 h (Fig. 10). The low-frequency band encloses the principal harmonic tidal constituents (M_2 and S_2) plus a residual current flow (much less energetic than the tidal current). Since the spectral resolution was 0.0148 cph, it was not possible to separate the individual contribution of the semi-diurnal tidal components M_2 and S_2. The high-frequency band encloses shallow water tidal harmonic constituents and internal soliton current pulses. In the velocity time series these last current components occur as aperiodic short-period nonlinear fluctuations, in the form of KDV solitons, and for that reason they became unresolved by Fourier analyses. To appreciate the forcing contribution of each NIW a simple data processing method was developed (Quaresma, 2006).

This method comprises the removal of significant short-period velocity anomalies, induced by each NIW current pulse, from the original time series. For this purpose, the original velocity time series was differentiated, with resulting high signal magnitudes corresponding to rapid velocity variations (these were the NIW current pulses). To the remaining signal (velocity time series

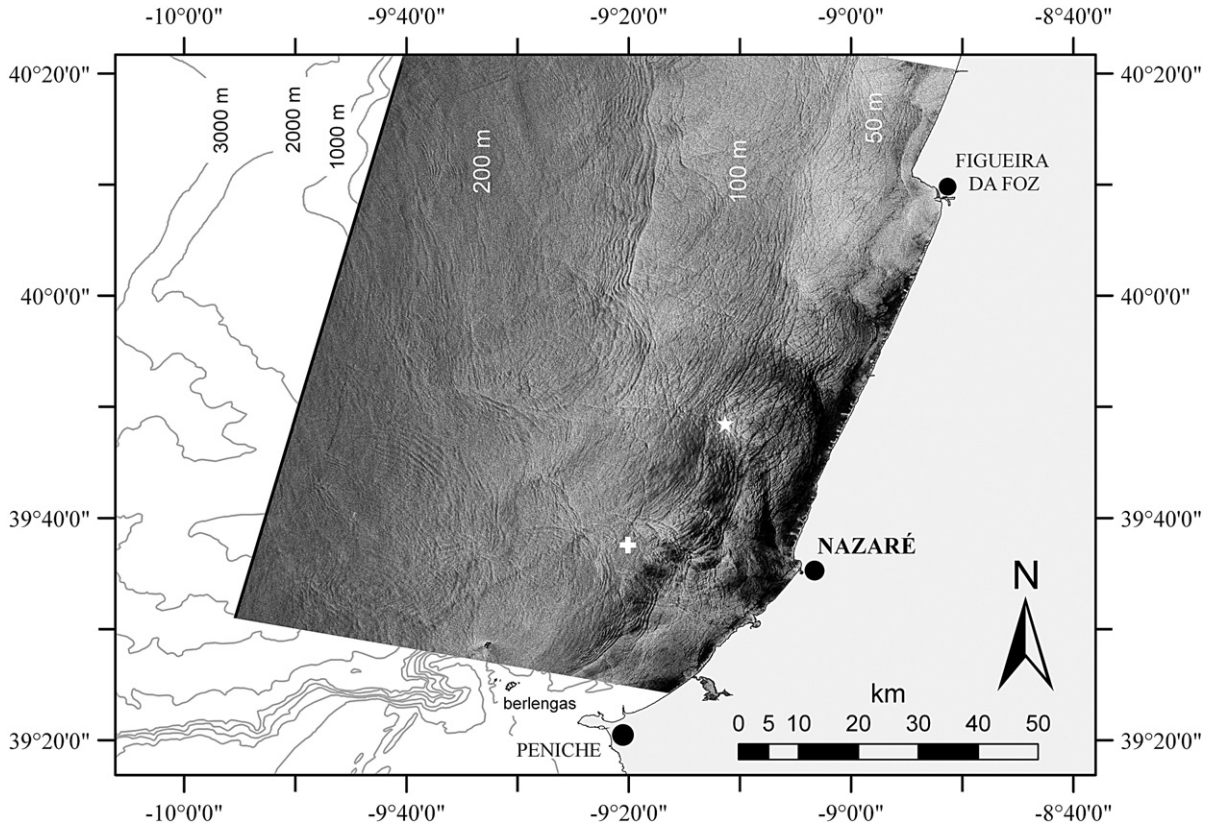


Fig. 7. ENVISAT ASAR image taken during the experiment period (30AUG2004 — 10 h 54 min UTM). The image shows sea surface manifestations of both SB-NIW and C-NIW trains, as well as their mutual crossing-over at the Portuguese continental mid-shelf (north of the canyon). *Station A* is represented by a cross and *Station B* by a star. The NIWs interpretation of this image is presented in Fig. 8.

without the high-frequency anomaly values), a polynomial function was adjusted in order to reproduce the low-frequency variability (composed mainly by the semi-diurnal tidal current). Subtracting this variability from the original time series, each NIW current pulse became isolated, in an original KDV-type format. This process was validated by the spectral representation of the recovered tidal current, which shows a cutoff period around 5 h, where the energy decreases two orders of magnitude from low to high frequencies (Fig. 11). This decomposition method allows a better characterization of both frequency domains:

1) Low-frequency. The semi-diurnal tidal current is the most important variability present in the velocity records. This current is polarized along the SW–NE direction (almost parallel to the bathymetry), with the maximum velocity magnitude felt in the upper layer (~ 0.12 m s^{-1}). Near the bottom, this profile presents a logarithmic decay (to a maximum bottom velocity magnitude of about 0.06 m s^{-1}, at 0.4 mab), corresponding to a turbulent boundary layer, with an average height of about 2 m. Near the bottom the residual flow shows a very small variability, becoming almost negligible.
2) High-frequency. The shallow water tidal harmonic constituents revealed low variability, two orders of magnitude lower than the semi-diurnal, similar to background noise. Since the internal soliton pulses occurred as nonperiodic fluctuations of the current, they appear in the spectra as part of this unresolved background noise.

6.4. NIW characterization

The temperature profile records show the propagation of different solitons as nonlinear thermocline fluctuations, with amplitudes varying from 10 m to almost 30 m and periods from 8 to 25 min. The SAR image reveals that these NIW can be grouped in two different propagation directions, resulting from different NIW generation spots: continental shelf-break (SB-NIW) and Nazaré upper canyon (C-NIW). The current profile processing allowed the isolation of each soliton

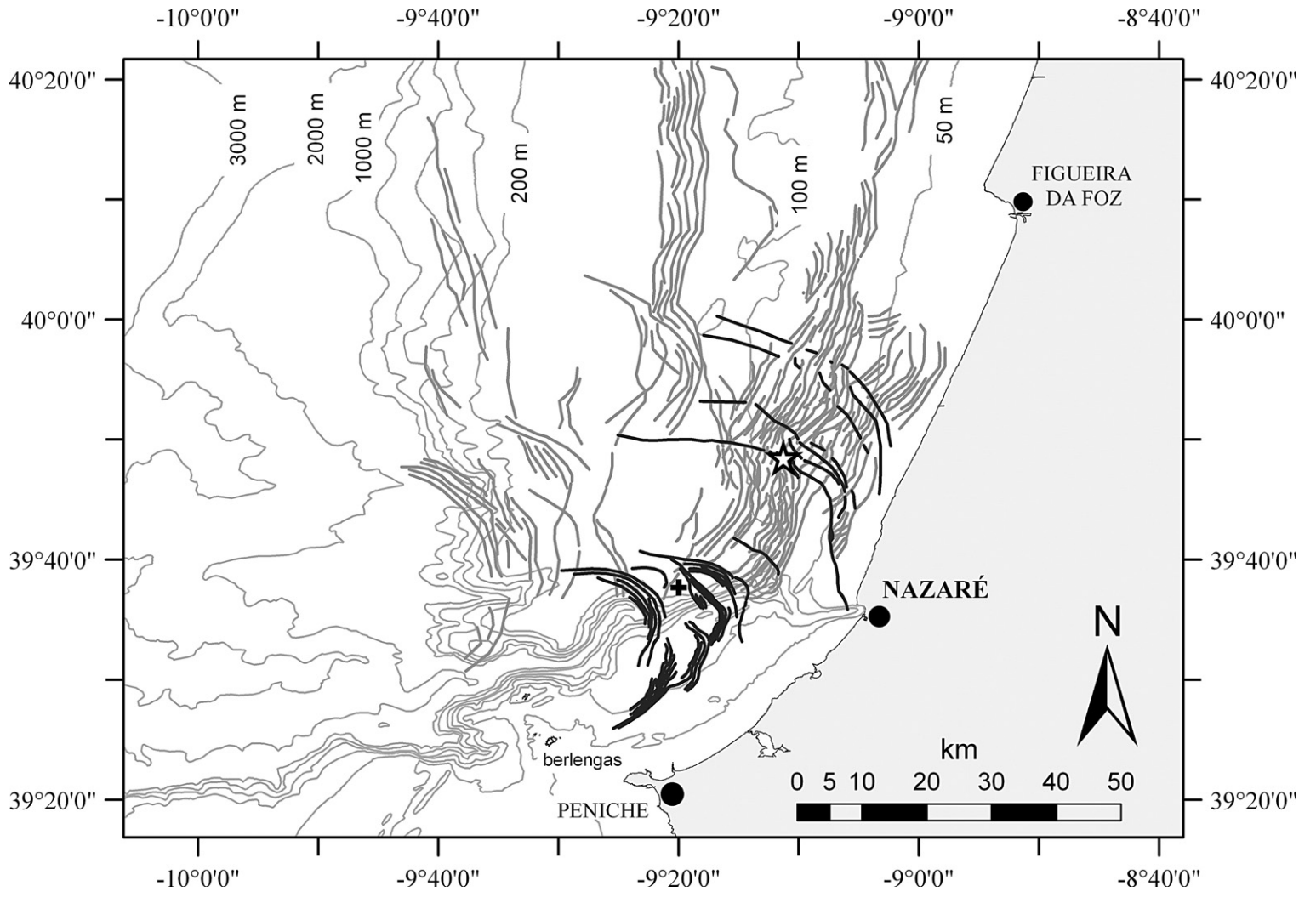


Fig. 8. Identified sea surface manifestations of NIW solitons from the ENVISAT ASAR image (Fig. 7). The SB-NIWs solitons are represented in light grey bold lines and the C-NIWs solitons in black bold lines.

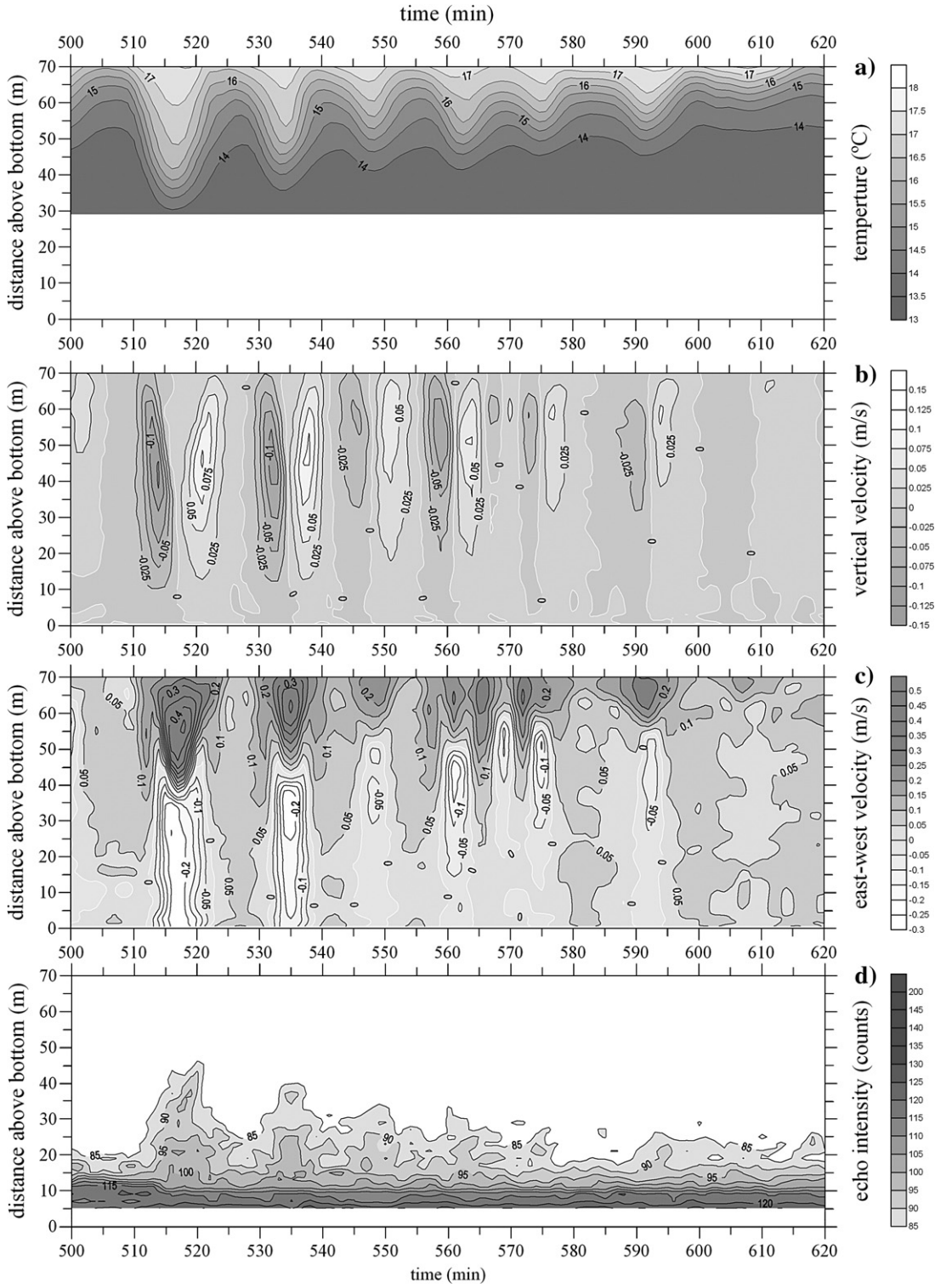


Fig. 9. NIW packet recorded at *Station B*, from 21:45 h to 23:45 h UTC (August 29th, 2004). a) temperature profile time series (°C); b) vertical velocity profile time series (m s^{-1}); c) east–west velocity profile time series (m s^{-1}); d) 300 kHz ADCP echo intensity profile time series (*in* counts). This time section corresponds to hour 8–10 in the Fig. 14.

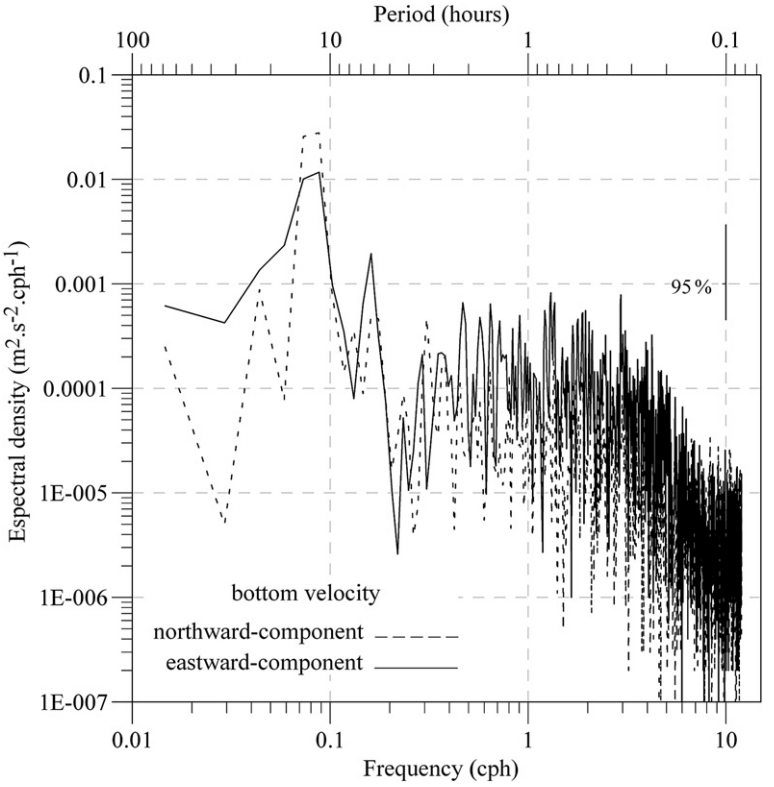


Fig. 10. Spectral density of the eastward and northward components of bottom current (1 mab), recorded by the 1200 kHz at *Station B*. Frequency in *cycles per hour* (cph). The series duration is ~2.8 days and sampling interval of 1 min (N=4045). The *frequency resolution* is 0.0148 cph, with 2 degrees of freedom. The vertical bar gives the 95% level of confidence.

pulse, and as such, the identification of the direction of propagation and magnitude of each NIW. A simplified two-layer system was assumed, based on the water column stratification (see Section 5.2). We used a NIW propagation model representing the evolution of a KDV equation solution (Liu et al., 1998; Apel, 2003). Briefly, this 2D model shows that there is an orbital velocity field associated with each nonlinear pycnocline fluctuation (in the form of a KDV solution), where the horizontal velocity varies in sign from the upper layer to the lower layer and the vertical velocity presents its maximum magnitude at the density interface. The direction of the orbital velocity (horizontal component) in the upper layer corresponds to the propagation direction of the associated internal solitary wave (for the case of depression solitons in a system where the upper layer is thinner than the lower one).

Fig. 12b shows the representation of the velocity pulses on a rose diagram for the velocity time series at 10 m depth (70 mab). The same two main groups of NIW trains identified in the SAR image can be identified. These are: 1) strong current pulses with an east–southeast direction, corresponding to the SB-NIW; 2) strong current pulses with east–northeast direction, corresponding to the C-NIW. These results reveal that the solitons had their principal propagation component in the direction perpendicular to the bathymetry, recording eastward velocity amplitudes up to 0.45 m s^{-1} (Fig. 9c).

A similar analysis was performed to the processed velocity time series at 1 mab. The rose diagram of these bottom soliton current pulses shows the same propagation orientations (Fig. 12a), but with opposite directions (in agreement with the KDV evolution model). However, the same diagram reveals that the strongest bottom current pulses have a west–southwest direction, corresponding to the C-NIW orientation path. These high magnitude current pulses (up to 0.2 m s^{-1}), observed upon the sea floor, are in accordance with the KDV model, as a result of higher amplitude short-period pycnocline fluctuations (also observed in the Fig. 9a,c).

These results show that the high amplitude solitons, observed in the temperature profiles, are in fact generated in the Nazaré upper canyon. Fig. 9d shows that these C-NIWs are also associated with strong increases of the near bottom ADCP backscattered echo,

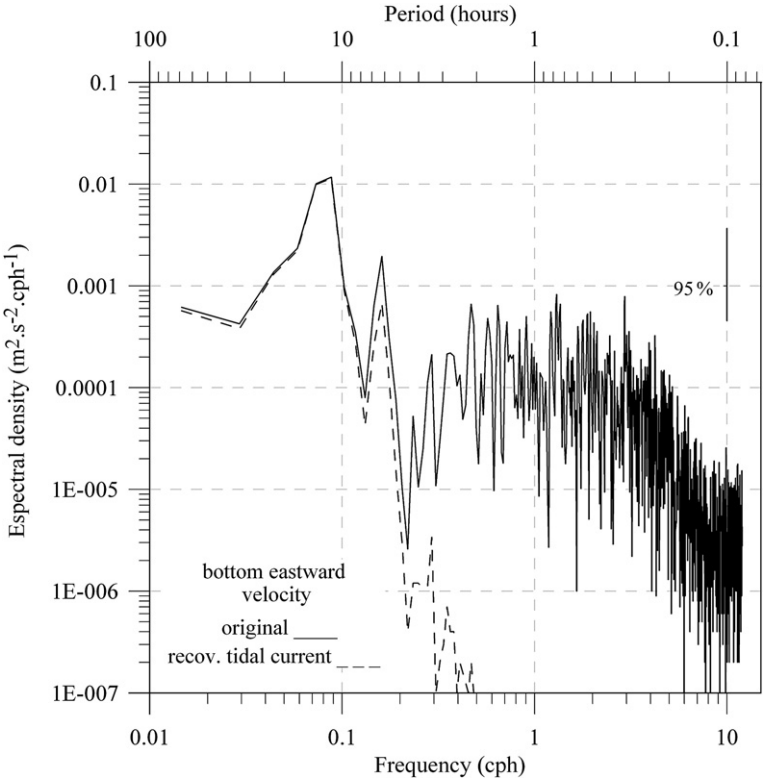


Fig. 11. Spectral density of the original eastward components vs. spectral density of the recovered eastward tidal current series (obtained by the developed filtering method in Section 6.3). The series duration is ~2.8 days and sampling interval of 1 min (N=4045). The *frequency resolution* is 0.0148 cph, with 2 degrees of freedom. The vertical bar gives the 95% level of confidence.

suggesting that their strong bottom current pulses forced the resuspension of local sediment. The next section will evaluate this C-NIW sediment resuspension potential.

7. Impacts of NIWs on the bottom sedimentary cover

7.1. Turbidity observations

The nephelometry profiles obtained during the experiment show interesting aspects in the spatial distribution of the suspended sediment. Along the C-NIWs track the water column turbidity shows an average value of about 0.25NTU and evidences a bottom nepheloid layer (BNL) over the mid-shelf (Fig. 13), with values of about 1.0NTU. This layer is 10 to 15 m thick, extending from the 130 m to the 60 m isobath and with maximum expression over *Station B*, where the bottom turbidity reaches 1.4NTU. This behavior seems to disappear over the shallower CTD station (~50 m depth), where the turbidity is redistributed along the profile, with an average value of 0.5NTU and a maximum over the thermocline (15 m depth).

The echo intensity recorded by the upward-looking ADCP (*Station B*) also reveals the same nepheloid structure along the experiment period. The strong backscattered echo from the first 10 mab shows the existence of the BNL. On top of this layer, the same time series shows short-period increases, in phase with the passage of the strong NIWs (Fig. 9a,d). These short-period echo variations are proportional to the solitons amplitude, suggesting that pumping of sandy particles reaches up to levels above the BNL (up to 40 mab). This supposition is in agreement with the high settling velocity of the sand particles (~0.02 m s^{-1}) and the rapid echo decrease after the passage of each strong thermocline fluctuation (NIW). It is also important to notice that the sand grain size agrees with the high backscattering coefficient for the 300 kHz ADCP signal frequency.

7.2. Bottom stress estimates

During the observation period the near bottom current was mainly caused by the low-frequency circulation,

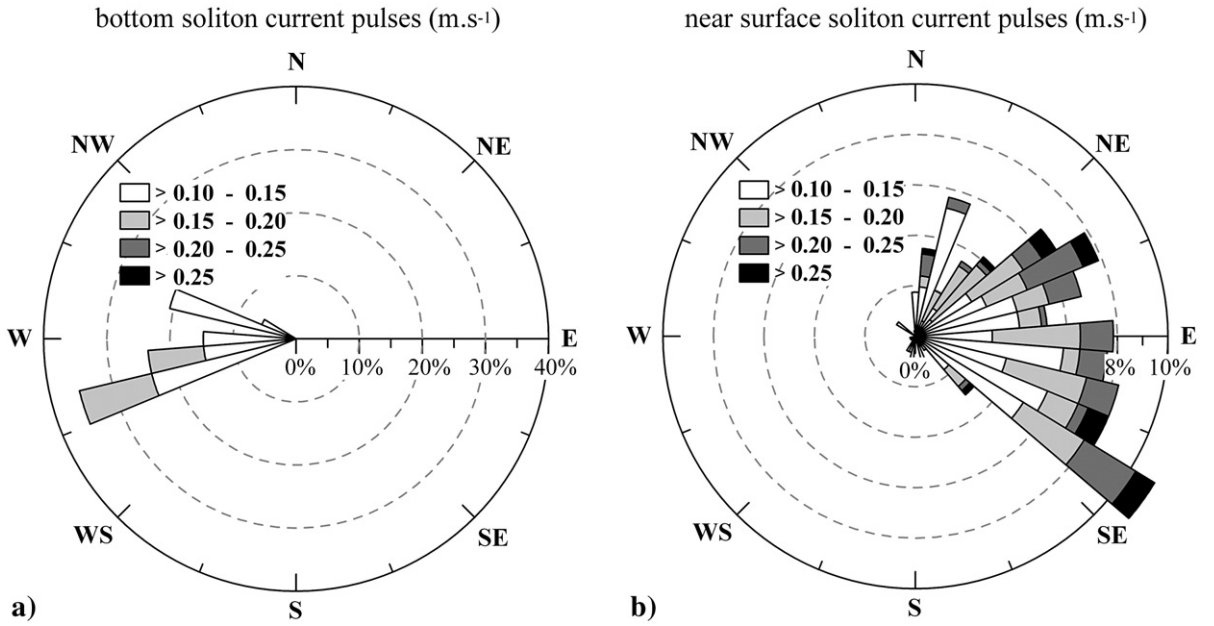


Fig. 12. Soliton current pulses distribution frequency, recorded by the ADCPs at *Station B*. a) bottom soliton current pulses (1 mab); b) near surface soliton current pulses (70 mab). Note the direction of the two strongest near surface pulses, that corresponds to the C-NIWs and SB-NIWs orientation path, and the direction of the strongest bottom pulses, that corresponds to the C-NIWs orientation path.

tides and by the strong NIW current pulses (forcing temporary steady flows during 1 to 2 tens of minutes). Due to the low energy surface wave regime, found during the experiment, the associated near bottom wave orbital velocity (at 80 m depth) should be negligible and is not considered here. The bottom current velocity generates friction near the seabed. This friction gives rise to a turbulent boundary layer, where the velocity U varies with the height z, above the bed, according to the logarithmic velocity profile,

$$U(z) = \frac{u_*}{k} \ln\left(\frac{z}{z_0}\right) \quad (1)$$

where u_* is the *friction velocity*, z_0 the *bed roughness length* and k the *von Karman's constant* (~ 0.4). The frictional force exerted by the current per unit area of bed (N m^{-2}) is expressed in terms of the bed shear stress, τ_0, related to the friction velocity by

$$\tau_0 = \rho u_*^2 \quad (2)$$

7.2.1. The logarithmic profile

In the experiment, the bottom velocity profile was measured by the downward-looking ADCP. The characteristics of the current profile, in the bottom boundary layer, were determined using a separate analysis for each one of the two frequency components, identified in the spectra and separated by the developed decomposition method (see Section 6.3). The low-frequency component (mainly composed of the tidal current) shows a well developed *log-profile*, in the first 2 mab. On the other hand the strong current pulses induced by the NIWs present a uniform bottom current profile, suggesting a very thin *bottom shear layer* (as expected at high frequency), which was probably out of range for the downward-looking ADCP measurements (*shear layer* height <0.4 mab).

7.2.2. The bed form roughness

The *bed form roughness* was obtained by fitting a logarithmic solution to the mean current profile, which was obtained after removing the short-period NIW pulses from the current measurements (see Section 6.3). The value obtained is about 0.5 mm, which is very similar to the value found by Soulsby (1983) for unrippled sandy sediments (0.4 mm).

7.2.3. The friction velocity

The *friction velocity* (u_*) associated to the low-frequency current was also obtained from the fit of a logarithmic solution to the recovered tidal current profile series (see Section 6.3). The estimation of the *friction velocity* induced by the NIW current pulses follows a different approach. Assuming that the top of the corresponding *logarithmic bottom shear layer* was located near 0.4 mab (the nearest bottom velocity record), the

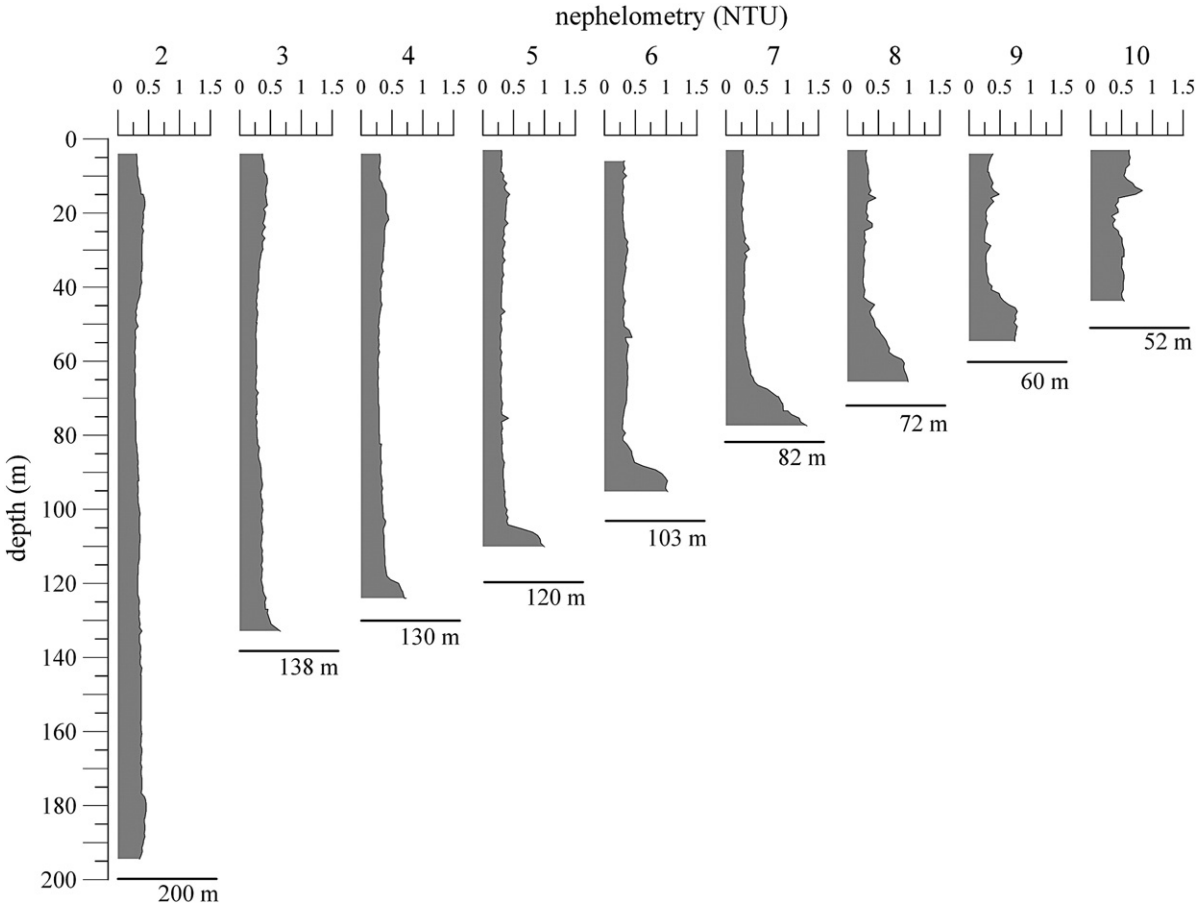


Fig. 13. CTD nephelometry profiles along the C-NIWs track (from generation to breaking zone). The location of each CTD profile is presented in Fig. 4. The hydrographic section survey was performed from 4:00 to 08:00 h UTM (August 31st, 2004). Note the existence of a bottom nepheloid layer (BNL), along the mid-shelf, with a maximum turbidity at the observational *Station B* (corresponding to the CTD profile no. 7).

induced u_* was obtained by solving Eq. (1), using the *bed form roughness* previously calculated (0.5 mm). This assumption leads to an underestimation of the friction velocity induced by the NIWs, since the thickness of the respective bottom boundary layer should be smaller than the one adopted, and therefore promoting higher u_*.

7.2.4. The bed shear stress

The combined effect of the *bottom shear stress* forced by the low-frequency residual flow (τ_{rc}), tidal current (τ_{tc}) and NIW current pulses (τ_{NIWc}) is assumed to be the result of a simple linear addition of each instantaneous single stress,

$$\tau_b = \tau_{rc} + \tau_{tc} + \tau_{NIWc} \quad (3)$$

This assumption is based on the capability to decompose the observed current velocity into these 3 linear components (see Section 6.3). Each stress constituent was obtained by applying Eq. (2) to the corresponding *friction velocity*.

7.3. Sediment resuspension due to NIWs

To estimate the potential for local sediment resuspension, by the combined effect of low- and high-frequency bottom shear stress, calculations of *mobility Shields parameter* were made. This parameter is obtained from the ratio of the force exerted by the bed shear stress (acting to move a grain on the bed) to the submerged weight of the grain counteracting this force (Soulsby, 1997):

$$\theta = \frac{\tau_b}{(\rho_s - \rho_w)gd} \quad (4)$$

where τ_b is the *bed shear stress*, g is the *gravitational acceleration* (9.81 m s^{-2}), ρ_s is the *grain density* (assumed to be the quartz density, 2650 kg m^{-3}), ρ_w is

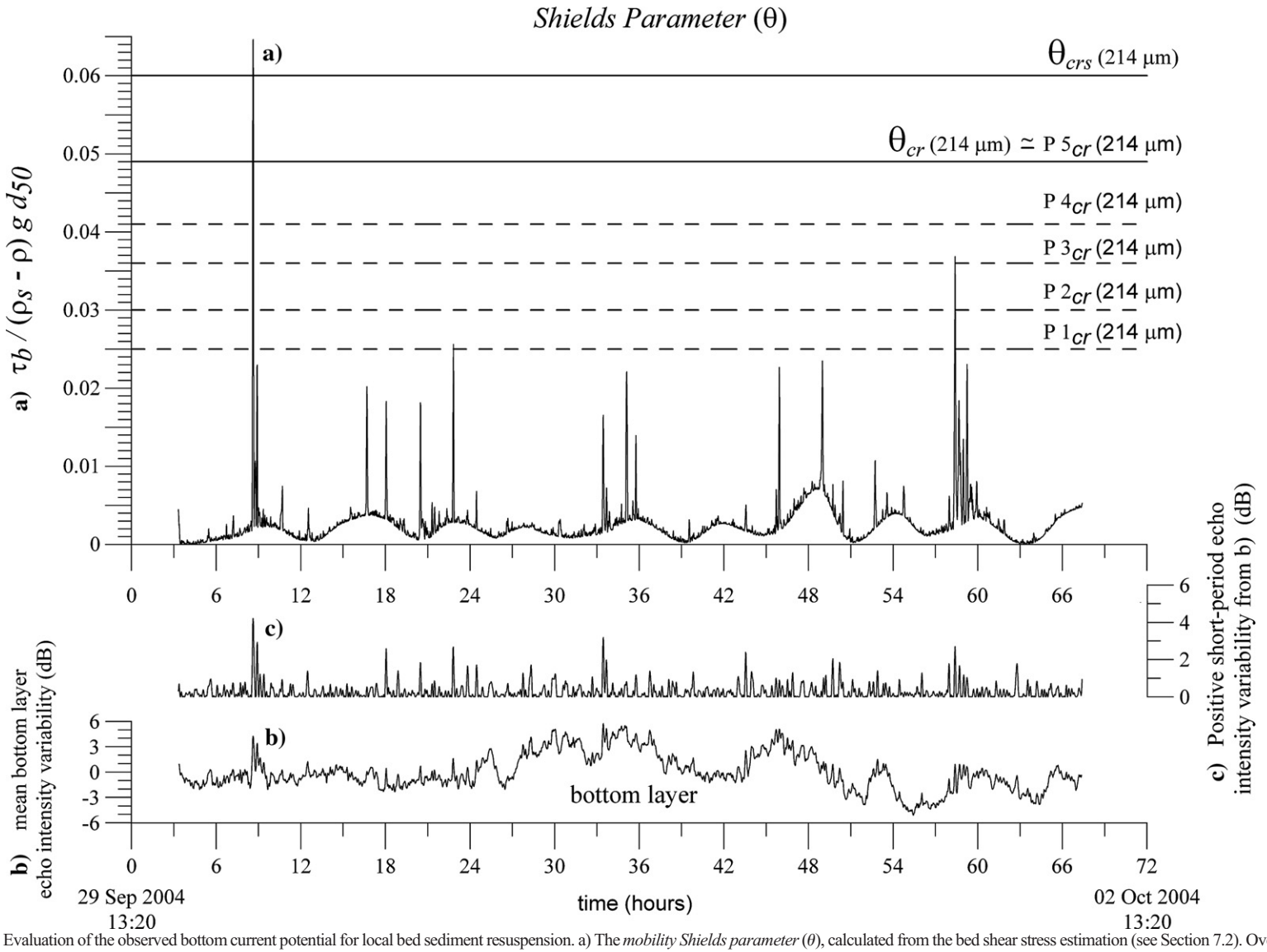


Fig. 14. Evaluation of the observed bottom current potential for local bed sediment resuspension. a) The *mobility Shields parameter* (θ), calculated from the bed shear stress estimation (see Section 7.2). Overlay of the critical *Shields parameter* level for mobilization of the local dominant sediment grain size, θ_{cr} (214 μm), the critical *Shields parameter* level for the suspension of the same grain size, θ_{crs} (214 μm) = 0.060, as well as the *probability mobility critical levels* (P), defined in the Delf Hydraulics report (1972) as: P1 = occasional particle movement at some locations; P2 = frequent particle movement at some locations; P3 = frequent particle movement at many locations; P4 = frequent particle movement at nearly all locations; P5 = frequent particle movement at all locations (corresponding to the *mobility threshold bed shear stress*, θ_{cr}). b) Mean 300 kHz ADCP echo intensity variability measured above the BNL (10–30 mab). c) Positive short-period variability from b), identified by high-band pass filtering (cutoff period of 0.5 h).

the *bottom water density* (observed during the experiment, ~1027 kg m^{-3}) and d is the *particle diameter*. The *mobility Shields parameter* was calculated from the estimated combined *bed shear stress* (see Section 7.2.4) assuming d=214 μm, that corresponds to the median grain size (d_{50}) found in the local seabed sediment samples (see Section 5.1).

The *threshold bed shear stress* (bed shear stress value above which the seabed sediment grains begin to move) was obtained by the following formula (Soulsby and Whitehouse, 1997),

$$\theta_{cr} = \frac{0.3}{1 + 1.2D_*} + 0.055[1 - \exp(-0.02D_*)] \quad (5)$$

where D_* is the dimensionless grain size given by,

$$D_* = \left[\frac{g(s-1)}{v^2}\right]^{1/3} d \quad (6)$$

where v is the *kinematic viscosity of water* (1.16×10^{-6} for T=15 °C and S=35, Siedler and Peters, 1986) and $s = \rho_s / \rho_w$. The calculated values for the median grain size are D_* (214 μm)=4.83 and θ_{cr} (214 μm)=0.049.

The obtained time series of *mobility Shields parameter* is presented in Fig. 14, together with the median grain size *threshold bed shear stress*, as well as with a *threshold bed shear stress* for the suspension of the same dominant sediment, θ_{crs} (214 μm)=0.060. This last parameter corresponds to the value presented by Van Rijn (1989) as the lower limit of the *threshold bed shear stress* for D_* ~5. Fig. 14 reveals that during the strongest C-NIW pulse (near hour 9), the *Shields parameter* exceeded both mobility and suspension critical levels. This indicates that strong C-NIW pulses are able to erode the local sediment from the bottom, bring it in suspension. As the sand grains are quite heavy, with settling velocity of 0.02 m s^{-1}, they will fall quickly after the C-NIW forcing stops. This behavior is indeed suggested in Fig. 9d, which shows a rather good correlation between the lower layer echo intensity variation and the record of two strong NIW pulses (Fig. 9a,d).

Calculation of the absolute backscattering strength in dB (Sv) was performed following Deines (1999) in order to quantify the echo intensity variation. After this step, the echo profile series was integrated from 10 to 30 mab (corresponding to a region just above the BNL) and the resulting values compared with the bottom shear stress (Fig. 14a,b). To identify the high-frequency variability from this series, a high-band pass filtering was performed (with a cutoff period of 0.5 h). The resulting positive short-period variability is presented in Fig. 14c. A quick look at this figure shows significant correlation between the Shields parameter and the high values of short-period echo variations (Fig. 14a,c). This means that there is evidence of short-period variability in phase with NIW pulses, reaching neither the *threshold bed shear stress* for the suspension nor the *threshold bed shear stress* for mobilization. The same *Shields parameter* time series was compared with *probability mobility critical levels* (P), defined in the Delft Hydraulics report (1972) in order to find out if this echo increases were also due to the forcing of the smaller NIWs. The results indicate that the majority of these NIWs rest just below the mobility threshold probability region (Fig. 14a). Even if the bottom shear stress induced by the NIWs was underestimated (see Section 7.2.3), it is not expected that these lower shear stresses can erode the seabed sediment. Nevertheless, the current observations showed that almost every NIWs induce strong vertical velocities, that could interact with the observed BNL. This means that the passage of each soliton (C-NIWs and SB-NIWs) is pumping the near bottom suspended sediment to levels above the BNL, therefore contributing for the short-period echo increase in the integrated vertical region.

8. Conclusions

The presented observations show the propagation of strong NIWs over the western Portuguese mid-shelf. These internal waves, generated over the Nazaré submarine canyon (C-NIW) seem to be the result of an interaction between the semi-diurnal tidal current and the upper canyon rim at the position 39°37′N/009°23′ W. This position is located near the coast (~25 km offshore) and therefore the produced C-NIWs propagate shoreward directly to the mid-shelf (depths <120 m). The recorded data analyses revealed a repeated crossing-over event between these C-NIWs and numerous solitons which propagate from the shelf-break (SB-NIW). These SB-NIWs have already been reported by other authors (Jeans, 1998; Jeans and Sherwin, 2001a,b; Sherwin et al., 2002) as shoreward propagation NIW trains, losing energy along their path and arriving to the mid-shelf region with a significant decrease in amplitude and in current pulse magnitude. These characteristics were also observed in the present work, with the C-NIW showing higher amplitudes (reaching almost 30 m) and stronger short-period current pulses. Near the bottom, the C-NIW current pulses occurred every semi-diurnal period (corresponding each to 2 or 3 high amplitude solitons), varying from 0.1 to 0.20 m s^{-1} (during 10 to 20 min). Both echo intensity data and bottom shear

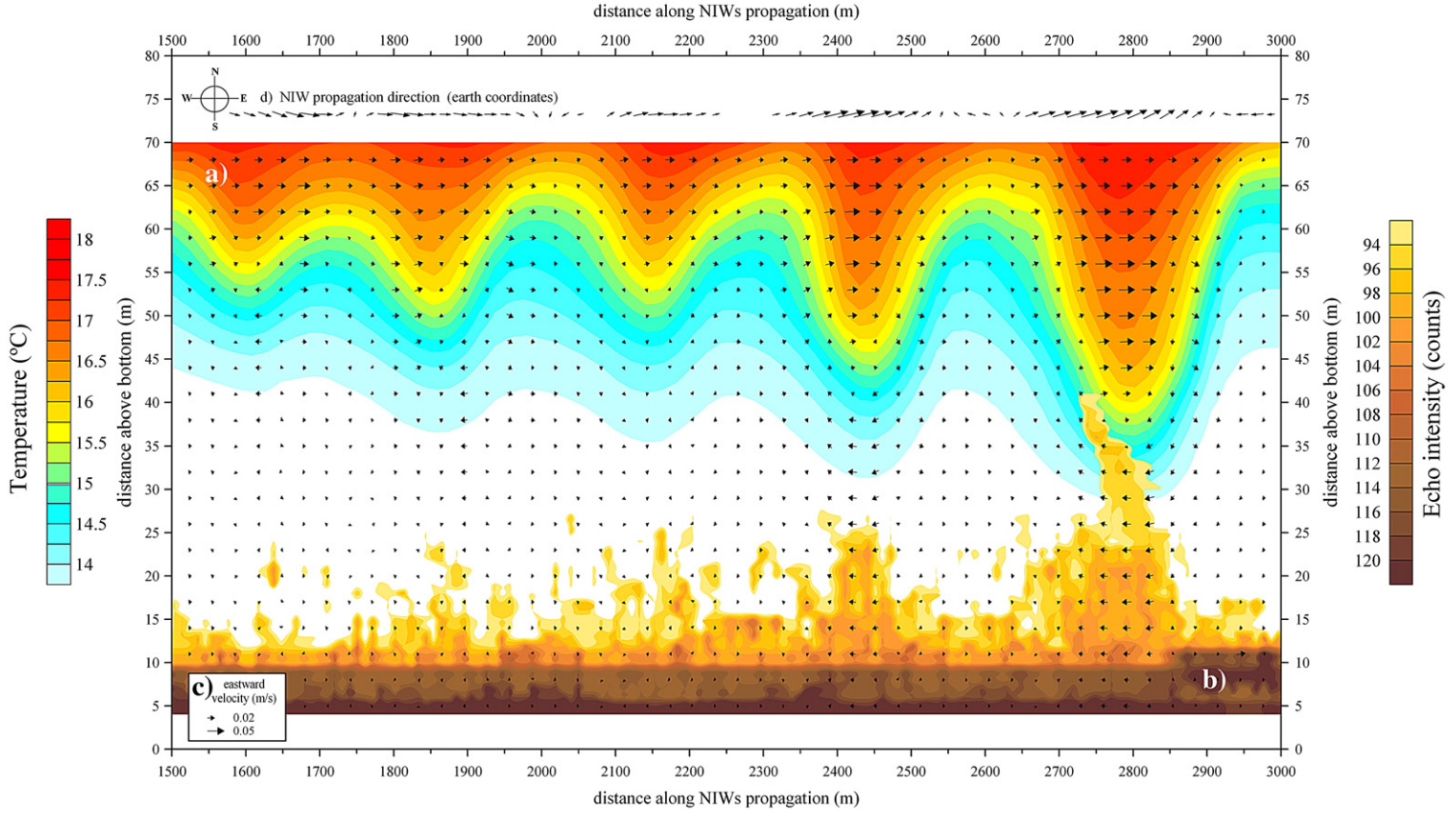


Fig. 15. *In-situ* NIW observations over *Station B* (2004 experiment). The figure shows the propagation of the first five NIWs represented in Fig. 9 (corresponding to the strongest NIW packet observed during the experiment). It is composed as an overlay of the following recorded series: a) temperature profile (°C), obtained by the thermistors chains; b) 300 kHz ADCP echo intensity (*in* counts); c) 300 kHz ADCP eastward velocity (as vectors). d) Representation of the short-period current velocity vectors (observed near the surface) showing the propagation direction of each soliton (see Section 6.4). All presented time series are converted in spatial series (along eastward NIW propagation), assuming a constant phase velocity of 0.34 m s^{-1} (estimated *in* Quaresma (2006)).

stress calculations show that only the stronger C-NIWs are capable of eroding and suspending the local sediment. After mobilization, the different settling velocities will separate the dominant sandy sediment (~93%) from the smaller fraction of silt and clay components (~6%), that will remain in suspension. This mechanism contributes to sustain the observed 10–15 m thick summer BNL. Both C-NIW and SB-NIW induce considerable vertical velocities (0.025–0.1 m s^{-1}) that interact with the BNL and increase its thickness, even if most did not contain enough bottom shear stress to erode the sediment from the seabed (Fig. 15).

The total observed period (~2.8 days) was too short to evaluate the impact of a typical upwelling jet over the sedimentary cover, but it is known that this flow plays an important role in transporting the bottom suspended sediment (15.6–0.98 μm) towards the south and the shore, in the direction of the canyon (Oliveira et al., 2007-this issue).

The observed NIW trains are periodic semi-diurnal features that persist from late spring time to mid-autumn, following the seasonal rise of the upper thermocline. There is a high spatial correlation between the C-NIW area of activity and the north canyon mid-shelf sandy-gravel deposit (Fig. 2). Over this deposit a peculiar structure on the surface of the bottom sedimentary cover was demonstrated by Rodrigues, A. (personal communication): one large depression was identified, lacking present day fine sand deposition and rich in relict particles (coarse sand and gravel), as shown by clean sand deposits (silt and clay <1%). These features are in agreement with the high energetic conditions induced by the C-NIW, especially over the depressed area. The results of the present work suggest that the C-NIWs are playing an important role in the sediment dynamics of the mid-shelf region. The evaluated forcing mechanism is supplying the summer BNL and therefore contributes to the bypassing of the fine shelf sediment to the canyon axis (transported by the summer upwelling jet). The Nazaré canyon generated NIWs are therefore complementing the winter storm swell in forcing the erosion of fine sediments at mid-shelf depths.

Future observations and data analysis are already planned in order to evaluate the role of the energy dissipated during NIW breaking processes, and its impact on the local inner shelf sediment and biological community.

Acknowledgements

This study has been supported by the EU EUROSTRATAFORM project, Contract EVK3-CT-2002-00079, program "Energy Environment and Sustainable Development". Remote sensing data was acquired and processed in the frame of the FCT project SPOTIWAVE-II (POCI/MAR/57836/2004) and AMAZING (PDCTE/CTA/49953/2003). The authors are grateful to the crew and scientific team of the Portuguese navy vessel *NRP Auriga*. Special thanks to the following colleagues: Jorge da Silva, João Caldas, Aurora Bizarro, Ana Santos, Manuel Marreiros and António Martinho who participated in the data measurements and scientific discussion.

References

Alpers, W., 1985. Theory of radar imaging of internal waves. Nature 314, 245–247.

Apel, J.R., 2003. A new analytical model for internal solitons in the ocean. J. Phys. Oceanogr. 33, 2247–2269.

Apel, J.R., Byrne, H.M., Proni, J.R., Charnell, R.L., 1975. Observations of oceanic internal and surface waves from the Earth Resources Technology Satellite. J. Geophys. Res. 80, 865–881.

Benney, D.J., 1966. Long non-linear waves in fluid flows. J. Math. Phys. 45, 52–63.

Bogucki, D., Dickey, T., Redekopp, L.G., 1997. Sediment resuspension and mixing by resonantly generated internal solitary waves. J. Phys. Oceanogr. 27, 1181–1196.

Cacchione, D.A., Drake, D.E., 1986. Nepheloid layers and internal waves over continental shelves and slopes. Geo Mar. Lett. 6, 147–152.

Cacchione, D.A., Southard, J.B., 1974. Incipient sediment movement by shoaling internal gravity waves. J. Geophys. Res. 79, 2237–2242.

Clemente, C., Beja, J., Coelho, E.F., 2000. Internal tide on Setúbal submarine canyon — normal mode oscillation. Proceedings of 3rd Symposium on the Iberian Atlantic Continental Margin, Faro, Portugal, pp. 167–168.

Da Silva, J.C., 1997. The role of surface films in ERS SAR signatures of internal waves on the Iberian Shelf. PhD Thesis, Southampton University, unpublished.

Da Silva, J.C., Ermakov, S.A., Robinson, I.S., Jeans, D.R., Kijashko, S.V., 1998. Role of surface films in ERS SAR signatures of internal waves on the shelf, 1, short-period internal waves. J. Geophys. Res. 103, 8009–8031.

Deines, K.L., 1999. Backscatter estimation using broadband acoustic Doppler current profilers. Oceans 99 MTS/IEEE Conference Proceedings, Seattle, Washington, USA, pp. 13–16.

Delft Hydraulics, 1972. Systematic Investigation of Two-Dimensional and Three-Dimensional Scour. Delft Hydraulics, The Nether lands. report M648/M863.

Dias, J.M.A., 1987. Dinâmica sedimentar e evolução recente da plataforma continental portuguesa setrentrional. PhD. Thesis, Lisbon University, 500pp, unpublished.

Duarte, J.F., 2002. Distribuição espacial dos sedimentos do canhão da Nazaré e plataforma adjacente. Proceedings of Assembleia Luso-Espanhola de Geodesia e Geofísica, Valência, Tomo III, pp. 1162–1666.

Fanjul, E., Gómez, B., Sánchez-Arévalo, I., 1997. A description of the tides in the Eastern North Atlantic. Prog. Oceanogr. 40, 217–244.

Fiúza, A.F.G., Macedo, M.E., Guerreiro, M.R., 1982. Climatological space and time variation of the Portuguese coastal upwelling. Oceanol. Acta 5, 31–40.

Fortunato, A., Pinto, L., Oliveira, A., Ferreira, J., 2002. Tidally generated shelf waves off the western Iberian coast. Cont. Shelf Res. 22, 1935–1950.

Huthnance, J.M., 1995. Circulation, exchange and water masses at the ocean margin: the role of physical processes at the shelf edge. Prog. Oceanogr. 35, 353–431.

Jackson, C.R., 2004. An Atlas of Internal Solitary-like Waves and their Properties, Global Ocean Associates, second edition. February 2004, available on-line, http://www.internalwaveatlas.com/.

Jackson, C.R., Apel, J.R., 2002. An Atlas of Internal Solitary-like Waves and their Properties, Global Ocean Associates. available on-line, http://www.internalwaveatlas.com/.

Jeans, D.R.G., 1998. A non-linear internal tide on the Portuguese Shelf. Ph.D. Thesis, University of Wales, Bangor, unpublished.

Jeans, D.R.G., Sherwin, T.J., 2001a. The variability of strongly non-linear solitary internal waves observed during an upwelling season on the Portuguese Shelf. Cont. Shelf Res. 21, 1855–1878.

Jeans, D.R.G., Sherwin, T.J., 2001b. Energetics of non-linear internal waves on the Portuguese Shelf. J. Mar. Res. 59, 327–353.

Jorge da Silva, A., 1992. Dependence of upwelling related circulation on wind forcing and stratification over the Portuguese northern shelf. ICES CM2/C 17 12pp.

Jouanneau, J.M., Weber, O., Drago, T., Rodrigues, A., Oliveira, A., Dias, J.M.A., Garcia, C., Schmidt, S., Reyss, J.L., 2002. Recent sedimentation and sedimentary budgets on the western Iberian shelf. Prog. Oceanogr. 52, 261–275.

Kantha, L.H., Tierney, C.C., 1997. Global baroclinic tides. Prog. Oceanogr. 40, 163–178.

Lennet-Cody, C., Franks, P.J.S., 2002. Fluorescence patterns in high-frequency internal waves. Mar. Ecol., Prog. Ser. 235, 29–42.

Liu, A.K., Chang, Y.S., 1998. Evolution of nonlinear internal waves in the East and South China Seas. J. Geophys. Res. 103, 7995–8008.

Noble, M.A., Xu, J.P., 2003. Observations of large-amplitude cross-shore internal bores near the shelf break, Santa Monica Bay, CA. Mar. Environ. Res. 56, 127–149.

Oliveira, A., Vitorino, J., Rodrigues, A., Jouanneau, J.M., Dias, J.A., Weber, O., 2002. Nepheloid layer dynamics in the northern Portuguese shelf. Prog. Oceanogr. 52, 195–213.

Oliveira, A., Santos, A.I., Rodrigues, A., Vitorino, J., 2007e. Sedimentary particle distribution and dynamics on the Nazaré canyon system and adjacent shelf (Portugal). Marine Geology 246, 105–122 (this issue). doi:10.1016/j.margeo.2007.04.017.

Pires, H.O., 1989. Alguns Aspectos do Clima de Agitação Marítima de Interesse para a Navegação na Costa de Portugal. O Clima de Portugal, Fasc. XXXVII vol. 2. 34 pp.

Pombo, J., 2004. Sedimentos superficiais da plataforma continental portuguesa entre o Cabo Mondego e S. Martinho do Porto. MSc Thesis, Coimbra University, Portugal, 185pp, unpublished.

Puig, P., Palanques, A., Guillén, J., El Khatab, M., 2004. Role of internal waves in the generation of nepheloid layers on the northwestern Alboran slope: implications for continental margin shaping. J. Geophys. Res. 109, C09011.

Quaresma, L.S., 2000. Estudos Em Oceanografia Física - Maré Interna no Canhão Submarino da Nazaré. B.Sc Thesis, Évora University, Portugal, unpublished.

Quaresma, L.S., 2006. Observação de ondas internas não-lineares geradas sobre o canhão da Nazaré. M.Sc Thesis, Lisbon University, Portugal, unpublished.

Quaresma, L.S., Coelho, E.F., Rosa, L., Beja, J., 2000. Internal tide on Nazaré submarine canyon — head canyon measurements. Proceedings of 3rd Symposium on the Iberian Atlantic Continental Margin, Faro, Portugal, pp. 165–166.

Quaresma, L.S., Caldas, J.M., Vitorino, J., 2003. Corsed - Uma Plataforma Oceanográfica. Boletim do Instituto Hidrogr áfico-Hidromar vol. 73, 1–3.

Quaresma, L., Vitorino, J., Silva, J.C.B., 2005. Non-linear internal waves generated at Nazaré canyon: observations over the W Portuguese inner shelf. Geophysical Research Abstracts 7, 10135 EGU2005.

Sauvaget, P., David, E., Guedes Soares, C., 2000. Modeling tidal currents on the coast of Portugal. Coast. Eng. 40, 393–409.

Sherwin, T.J., Vlasenko, V.L., Stashchuk, N., Jeans, D.R., Jones, B., 2002. Along-slope generation as an explanation for some unusually large internal tides. Deep-Sea Res. I 49, 1787–1799.

Siedler, G., Peters, H., 1986. Numerical data and function relationships in science and technology, oceanography. Landolt-Börnstein 3, 260.

Small, J., 2002. Internal tide transformation across a continental slope off Cape Sines, Portugal. J. Mar. Syst. 32, 43–69.

Soulsby, R.L., 1983. The bottom boundary layer of shelf seas. Physical Oceanography of Coastal and shelf seas, B. Johns, p. 266.

Soulsby, R.L., 1997. Dynamics of marine sands. R. Soulsby and Thomas Telford Services Limited, London, ISBN:07277 2584 X. 249 p.

Soulsby, R.L., Whitehouse, R.J.S.W., 1997. Threshold of sediment motion in coastal environments. Proceedings of Pacific Coast and Ports'97 Conference. Christchurch,University of Canterbury, New Zealand, pp. 149–154.

Staquet, C., Sommeria, J., 2002. Internal gravity waves: from instabilities to turbulence. Annu. Rev. Fluid Mech. 34, 559–593.

Taborda, R., 1999. Modelação da Dinâmica Sedimentar na Plataforma Continenta Portuguesa. Ph.D. Thesis, Lisbon University, unpublished.

Van Rijn, L.C., 1989. Handbook of Sediment Transport by Currents and Waves. Delft Hydraulics, The Netherlands. Report H461.

Vanney, J.R., Mougenot, D., 1981. La plate-forme continentale du Portugal et les provinces adjacentes: analyse géomorphologique. Mem. Serv. Geol. Port. 28 145pp.

Vanney, J.R., Mougenot, D., 1990. Un canyon sous-marin du type "gouf": le Canhão da Nazaré (Portugal). Oceanol. Acta 13, 1–14.

Vitorino, J., Oliveira, A., Jouanneau, J.M., Drago, T., 2002a. Winter dynamics on the northern Portuguese shelf. Part 1: Physical processes. Prog. Oceanogr. 52, 129–153.

Vitorino, J., Oliveira, A., Joanneau, J.M., Drago, T., 2002b. Winter dynamics on the northern Portuguese shelf. Part 2: Bottom boundary layers and sediment dispersal. Prog. Oceanogr. 52, 155–170.

Vlasenko, V., Ostrovsky, L., Hutter, K., 2005. Adiabatic behavior of strongly nonlinear internal solitary waves in slope shelf areas. J. Geophys. Res. 110, C04006.

Wooster, W.S., Bakun, A., McLain, D.R., 1976. The seasonal upwelling cycle along the eastern boundary of the North Atlantic. J. Mar. Res. 34, 131–141.